(Received 11 November 2024, Accepted 3 January 2025, Scheduled 17 February 2025)

A High Isolation Four-Element MIMO Antenna for 5G n256-Band Satellite Communication and 6G Applications

Fanran Zhang, Chengzhu Du*, and Xu Wu

College of Electronics and Information Engineering, Shanghai University of Electric Power, Shanghai 200090, China

ABSTRACT: In the present work, a dual-band four-port multiple-input multiple-output (MIMO) antenna based on an FR4 substrate is designed, which can work in the frequency bands of 5G n256/n77/n78/n79 and 6G system. The MIMO antenna is composed of four orthogonally placed monopole antennas. Multiple sets of L-shaped branches and cross-shaped branches are added to improve the isolation among the antenna elements. The measured isolation is below −20 dB, and most of them can reach −30 dB within the operational frequency spectrum. The actual measurement results reveal that the two impedance bandwidths of the antenna are 420 MHz (1.95–2.37 GHz) and 4050 MHz (3.2–7.25 GHz), respectively, which can encompass the n256 band for 5G–6G satellite technologies (1.98–2.01 and 2.17–2.2 GHz), 5G n77/n78/n79 (3.3–4.2/3.3–3.8/4.4–5.0 GHz) and 6G band (6.425–7.125 GHz). At the same time, the antenna features a peak gain of 7.4 dB. The ECC value is below 0.0015, while the DG value exceeds 9.9999, showing good diversity performance. The data reveal that the designed dual-band quaternary MIMO antenna has good applications in the fields of 5G satellite communication and 6G systems.

1. INTRODUCTION

As wireless communication technology evolves at a fast pace, the fifth-generation (5G) mobile communication technology has been deployed on a large scale worldwide, bringing significant technological progress and application innovation. 5G technology not only significantly improves data transmission rate and network capacity, but also advances the widespread integration of emerging applications like internet of things (IoT), augmented reality (AR), and virtual reality (VR). Currently, the direct-to-cellular 5G satellite non-terrestrial networks (NTNs) and 6G become a hot point. 6G is expected to achieve higher transmission rate, lower delay, wider coverage, and higher connection density, and is expected to be commercially available around 2030 [1, 2].

As mobile communication technologies like 5G and 6G continue to develop, the utilization of spectrum in communication systems has become more diversified and complicated, resulting in a wide demand for multi-frequency MIMO antenna technology. The fusion of multi-frequency approaches and MIMO systems can greatly improve the efficiency of spectrum utilization, enhance the reliability of communication links, and achieve wider and deeper network coverage [3]. However, with space being limited, the distance between MIMO antenna elements is minimized, resulting in significant coupling among the units, which affects the signal propagation. Therefore, the challenge of minimizing coupling among multi-frequency MIMO antenna units while enhancing isolation has garnered significant attention.

At present, techniques frequently employed to decrease coupling in MIMO antenna units involve decoupling networks [4–7], diversity technique method [8–15], neutralization line method [16–18], defected ground structure method [19–25], and parasitic resonance structure method [26–35]. In [12], a four-element MIMO antenna has been proposed for the application in WLAN and Wi-Max frequency bands. The diversity technique method was used to achieve an impedance bandwidths of 3.0–4.4 and 5–6.6 GHz, and the isolation was greater than 18 dB. The antenna in [14] is suitable for 5G n77/n78 and X-band satellite communications, with isolation greater than 18 dB in the frequency range of 2.8–4.2 and 6.1–9 GHz. In [20], a four-element antenna is placed perpendicular to each other in the frequency ranges of 1.68–3.1 and 3.35–4.5 GHz, which can be applied to sub-6 GHz. The antenna of [26] adds an isolation structure to achieve a frequency range of 3.28–4.15 and 4.69–6.01 and an isolation greater than 19 dB. However, the above antennas are not connected to the ground. The antennas in [22, 23] have a connected ground; in [22] the antenna is compatible with 5G n79 and WiFi-6E bands; in [23] the antenna can be used for 5G-sub 6 GHz/n38/n41/n90 and WLAN bands. However, the isolation level between the two antennas is merely above 15 dB. In [27], the frequency bandwidths of the antenna are 1.85–3.63 and 5.07–7.96 GHz, including DCS, LTE2300/2500, Bluetooth, ISM, and WLAN bands. Ref. [28] proposed a dual-band antenna that can be applied to 5G n77/n78/n79, IEEE 802.11ac/ax, X-band/C-band wireless and satellite applications, and its isolation is greater than 20 dB. The antenna in [29] is made of denim and can be used in Bluetooth, IEEE 802.11 (a and b/g/n), WLAN, and WiMAX bands, but the isolation is only greater than 10 dB. Although the above three antennas have many application frequency bands, they are only two-element MIMO antennas.

* Corresponding author: Chengzhu Du (duchengzhu@163.com).

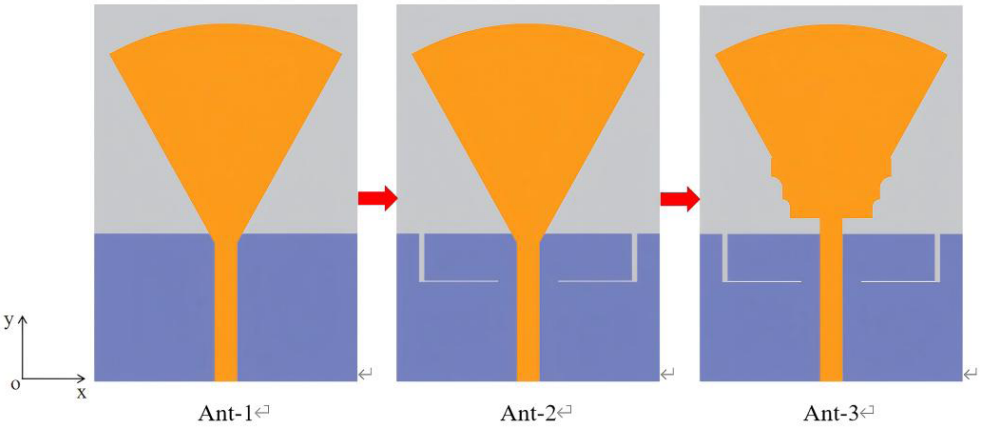

FIGURE 1. Design process of single element antenna.

With the rapid growth of direct-to-cellular 5G satellite non-terrestrial networks (NTN) and 6G systems, it is innovative to design a four-element MIMO antenna applicable to 5G n256/n77/n78/n79 and 6G systems.

The article presents a dual-band four-port MIMO antenna designed for 5G n256/n77/n78/n79 and 6G applications. The coupling among antenna elements is minimized through introducing isolation structures such as multiple sets of L-shaped branches and cross-shaped branches connected to the ground. Actual measurement results demonstrate that the antenna has a working bandwidth of 1.95–2.37 and 3.2–7.25 GHz; the isolation is below −20 dB; the envelope correlation coefficient (ECC) value is below 0.0015; the diversity gain (DG) value exceeds 9.9999. They meet the frequency band requirements of n256 5G satellite communication band (1.98–2.01 and 2.17–2.2 GHz), 5G n77/n78/n79 (3.3–4.2/3.3–3.8/4.4–5.0 GHz), and 6G (6.425–7.125 GHz).

The innovations of the antenna include: (1) The antenna covers the new n256 band for 5G-6G satellite technologies (1.98–2.01 and 2.17–2.2 GHz), 5G n77/n78/n79 (3.3–4.2/3.3–3.8/4.4–5.0 GHz), and 6G band (6.425–7.125 GHz) for 5G satellite communications and 6G applications. (2) The antenna is a four-element MIMO antenna with connected ground. This technology improves the capacity and spectrum utilization of the communication system, and improves the signal quality and anti-interference ability. (3) The antenna has high isolation better than 20 dB, and the ECC is less than 0.0015, while the DG is more than 9.9999, which has good diversity performance.

2. ANTENNA DESIGN

2.1. Single Element Antenna

As depicted in Fig. 1, the design evolution of the unit antenna takes place as follows. The proposed antenna is composed of a fan-shaped monopole with symmetrical L-shaped slots etched on the ground. The dielectric material for the antenna substrate is FR4, with a dielectric constant of 4.4, a loss tangent of 0.02, and a substrate thickness of 1.6 mm. The initial length of the symmetric L-shaped slots can be determined by the formula below:

$$L = \frac{C}{4f_c \times \sqrt{\varepsilon_{eff}}} \tag{1}$$

$$\varepsilon_{eff} \approx \frac{\varepsilon_r + 1}{2} \tag{2}$$

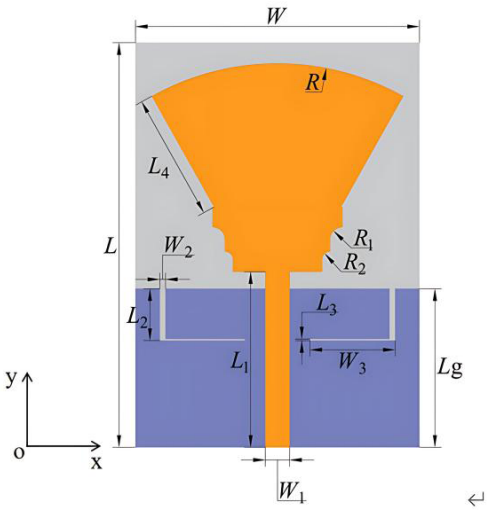

FIGURE 2. Structure of single element antenna.

In Fig. 2, a single element antenna structure is shown. The antenna's final design dimensions, obtained through the scanning and optimization of its parameters, are presented in Table 1.

TABLE 1. Parameters of the single antenna (in mm)

W	35	L	50	L_g	19.6
L_1	21.7	W_1	3	L_2	6.4
W_2	0.7	L_3	0.2	W_3	10.5
L_4	15.7	R	31.74	R_1	1.5
R_2	1				

Figure 3 is the S_{11} diagram of the single antenna at different stages. Ant-1 is a fundamental monopole antenna equipped with a fan-shaped patch, and its working bandwidth is 1.9–2.5 GHz, including the n256 satellite communication band. By etching a symmetric L-shaped groove on the ground, Ant-2 is obtained, functioning at two frequency ranges of 1.86–2.33 GHz and 3.32–3.73 GHz. Finally, in Ant-3, three stepped sides are added to the fan-shaped patch, and a dual-band antenna working at 1.84–2.33/3.16–7.45 GHz is obtained. It meets the requirements of 5G n256 n/77/n78/n79 and 6G applications.

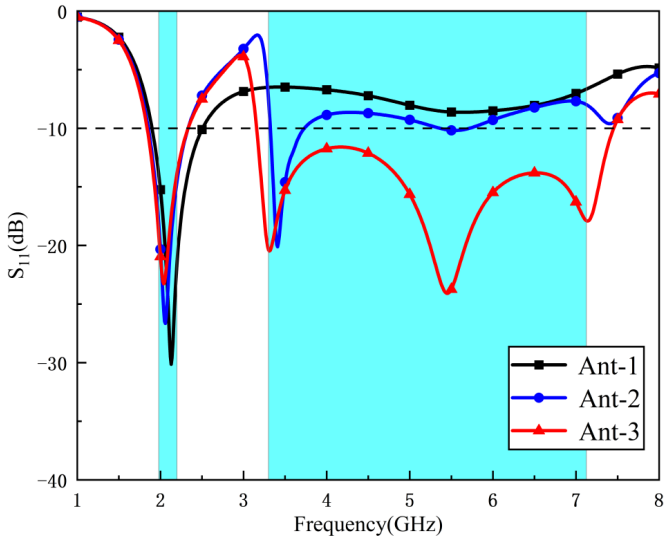

FIGURE 3. Comparison of S_{11} in different design stages.

2.2. Four-Element MIMO Antenna

Based on the monopole antenna, a dual-band four-element MIMO antenna has been conceived. The structural details and fabrication process are presented in Fig. 4. The suggested antenna is printed onto a FR4 dielectric substrate, sized at 100 mm×100 mm×1.6 mm. The design features four orthogonally oriented monopole antenna elements, with added isolation structures such as L-shaped branches and cross-shaped cross branches linked to the ground to lower the coupling among the antenna components. The antenna's geometry parameters, refined through simulation and optimization, are: $W_5 = 100$ mm, $L_5 = 100$ mm, $W_6 = 15$ mm, $L_6 = 66.9$ mm, $W_7 = 13.5$ mm.

2.3. Effects of Parameters

Figure 5 demonstrates how parameter W_2 affects the parameters of the antenna. As observed in Fig. 5, when W_2 gradually increases, the antenna has wider low-frequency bandwidth, and the change of isolation is small. Based on the above analysis, the final size of W_2 is 0.7 mm. Fig. 6 shows the effects of parameters W_3 on S-parameters of the antenna. In Fig. 6, as W_3 increases, the antenna has narrower low-frequency bandwidth, and the change of isolation is also small. Finally, $W_3 = 10.5$ mm was determined.

2.4. Decoupling Structure Analysis of the Antenna

Figure 7 shows the design workflow for the antenna decoupling structure, and Fig. 8 is the S-parameter simulation of the antenna with and without isolation structure. In Ant-I, four antenna elements are placed orthogonally without isolator and connected ground. The antenna's impedance bandwidths are 1.78–2.33 GHz and 3.21–7.22 GHz, and S_{21} is less than -20 dB, but S_{31} is only less than -15.5 dB. In Ant-II, a cross branch is added to reduce the coupling and connect the ground of four elements. The bandwidth of low frequency is wider; the S_{21} is less than -15.1 dB; the improvement of S_{31} is larger; the S_{31} is less than -18.4 dB. Finally, Ant-III is designed by adding four L-shaped branches on the Ant-II. The isolation can be further improved at high frequencies, and S_{31} are less than -21 dB at most of the frequency bands.

As shown in Fig. 9, the antenna's current distribution is presented for center frequencies of 2.1 GHz, 4.6 GHz, and 6 GHz. Excitation is applied to Port 1, and the remaining ports are linked to a 50 Ω load. At various frequencies, significant currents were detected in the excited antenna and isolation branches, highlighting the effectiveness of the isolation branches in minimizing coupling among antenna components.

From the above current diagram, it can be seen that the current is mainly concentrated on the cross-shaped branch, so the length of the branch L_6 is analyzed. As shown in Fig. 10 with the increase of L_6, the low frequency bandwidth increases; the high frequency range gradually moves to the high frequency direction; the impedance bandwidth decreases. When $L_6 = 66.9$ mm, the isolation is lower than -18 dB in the working bands. Therefore, the final size of L_6 is 66.9 mm.

3. EXPERIMENTAL VERIFICATION

3.1. S-Parameter

The comparison of the antenna's simulated S-parameters and measured results is presented in Fig. 11. The experimental data show that the trends in return loss fluctuations for both the measured and simulated results are largely in agreement. The measured impedance bandwidths of the antenna are 420 MHz (1.95–2.37 GHz) and 4050 MHz (3.2–7.25 GHz), respectively, which can cover the n256 satellite band (1.98–2.01 and 2.17–2.2 GHz), 5G n77/n78/n79 (3.3–4.2/3.3–3.8/4.4–5.0 GHz), and 6G (6.425–7.125 GHz). The measured S_{21} is less than -20.8 dB, and the measured S_{31} is less than -22.7 dB.

The analysis clearly indicates that although there are some variations in the S_{11} values between the measured antenna and simulated one, the trends are still observable, and the measured isolation is better than 20 dB. Through further error analysis, in the microwave frequency band, antenna processing accuracy and SMA head welding are the main reasons affecting the antenna performance.

3.2. Radiation Patterns

Figure 12 displays the MIMO antenna's measurement setup. Fig. 13 is the normalized radiation pattern of MIMO antenna. The E and H plane normalized patterns were respectively ac-

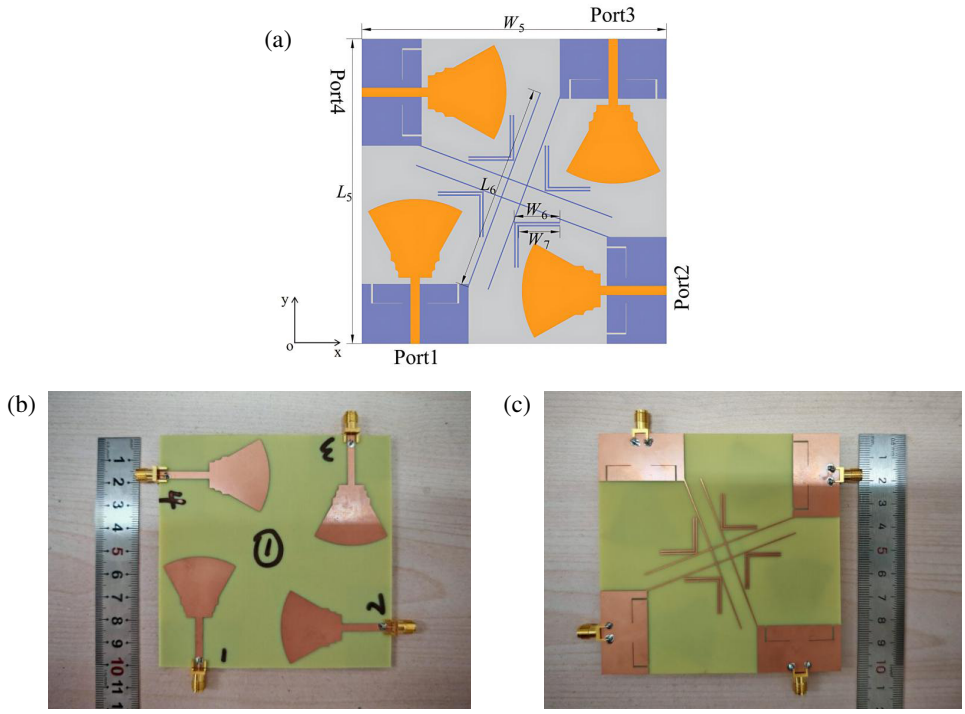

FIGURE 4. The structure and physical diagram of the proposed antenna. (a) Structure of the MIMO antenna. (b) Top view of the processed antenna. (c) Bottom view of the processed antenna.

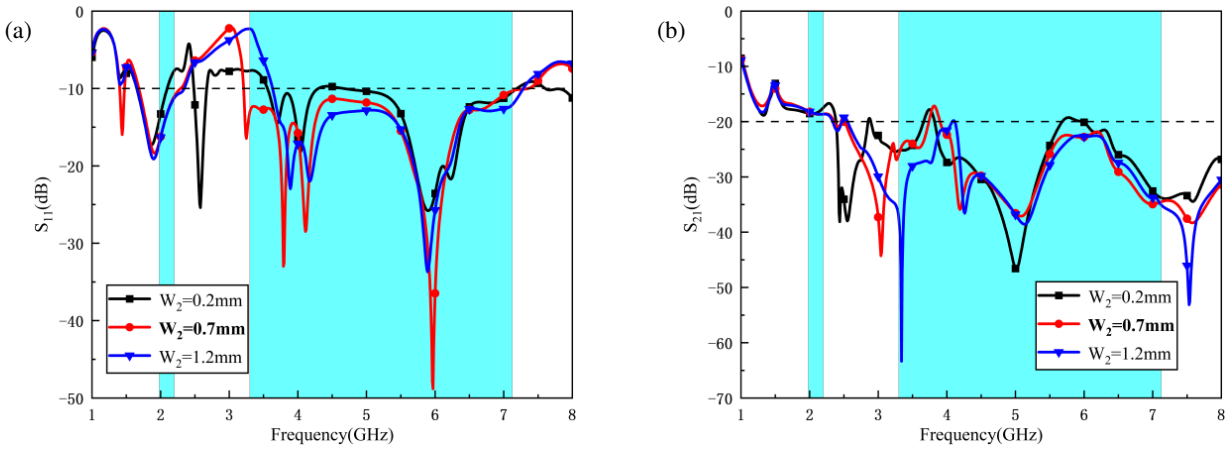

FIGURE 5. Effect of W_2 on S-parameter. (a) S_{11}. (b) S_{21}.

quired at 2.1 GHz, 4.6 GHz, and 6 GHz. As seen, the antenna's E-plane radiation pattern takes an '8' shape, indicating a well-defined two-way radiation mode; the H-plane radiation pattern basically satisfies the omnidirectional radiation characteristics and can transmit and receive signals in all directions. Although the pattern is slightly distorted at high frequencies, the overall trend remains unchanged. Overall, the antenna radiation performance is good.

3.3. Gain and Radiation Efficiency

Figure 14 shows the antenna's peak gain plot. The measured results reveal that at 2.1 GHz, 4.6 GHz, and 6 GHz, the gains are 4.2 dB, 6 dB, and 5.9 dB, respectively, achieving a maximum gain of 6.4 dB.

Figure 15 shows the comparison of radiation efficiency between simulation and test. The simulated radiation efficiency of the MIMO antenna is above 80% for both the operating bands.

3.4. ECC and DG

To facilitate a more intuitive discussion of antenna relationships within the study, envelope correlation coefficient (ECC) and diversity gain (DG) are generally used to measure the correlation between MIMO antennas in engineering. ECC can measure whether the coupling performance of the antenna is excellent. Better antenna performance is associated with a lower

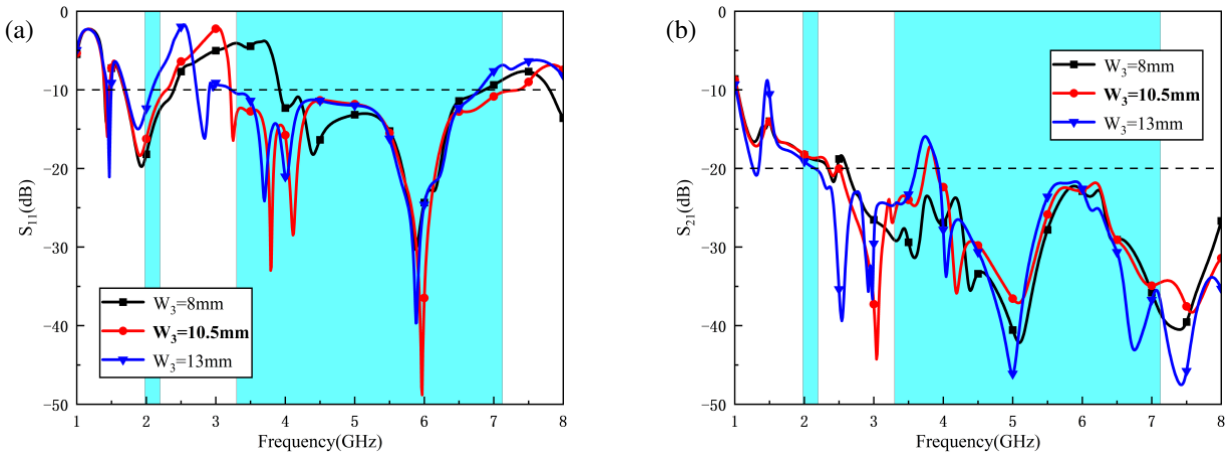

FIGURE 6. Effects of W_3 on S-parameter. (a) S_{11}. (b) S_{21}.

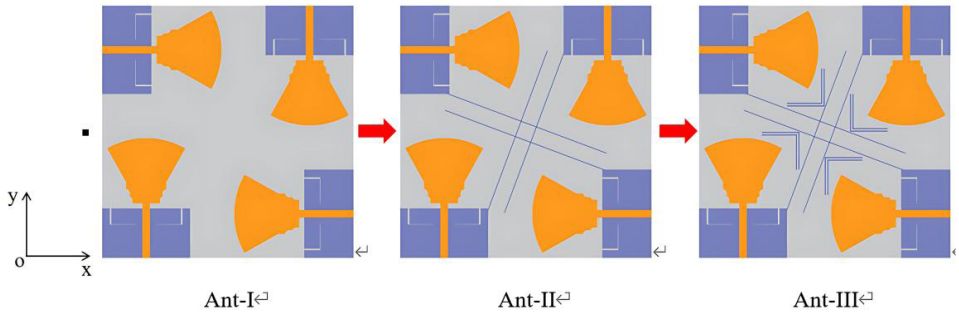

FIGURE 7. The design process of isolation structure.

TABLE 2. Comparison of antenna performance.

Ref.	No. of ports	Antenna size (mm^3)	Substrate material	Feeding method	Ground connection	Bandwidth (GHz)	Isolation (dB)	ECC	DG
[12]	4	64×64×1.6	FR4	Microstrip	No	3–4.4 5–6.6	>18	<0.03	>9.9
[14]	4	62×62×0.6	FR4	Microstrip	No	2.9–4.2 6.2–8.8	>18	<0.014	>9.9993
[20]	4	100×60×1.6	FR4	Microstrip	No	1.68–3.1 3.35–4.5	>22.5	<0.016	>9.9
[22]	4	48×48×1.6	FR4	Microstrip	Yes	4.45–5.2 5.95–7.15	>15	<0.005	>9.999
[23]	4	50×50×0.8	FR4	Microstrip	Yes	2.47–3.38 4.94–7.24	>15	<0.06	>9.95
[26]	4	68×68×0.8	FR4	Microstrip	No	3.28–4.15 4.69–6.01	>19	<0.0025	>9.999
[27]	2	40×30×1.6	FR4	Microstrip	Yes	1.85–3.63 5.07–7.96	>17	<0.003	>9.999
[28]	2	32×20×0.8	FR4	CPW	Yes	3.3–7.8 8.0–12.0	>20	<0.05	>9.9
[29]	2	100×60×1	Jeans	Microstrip	Yes	1.34–3.92 4.34–6.34	>10	<0.04	>9
Prop.	4	100×100×1.6	FR4	Microstrip	Yes	1.95–2.37 3.2–7.25	>21	<0.0015	>9.9999

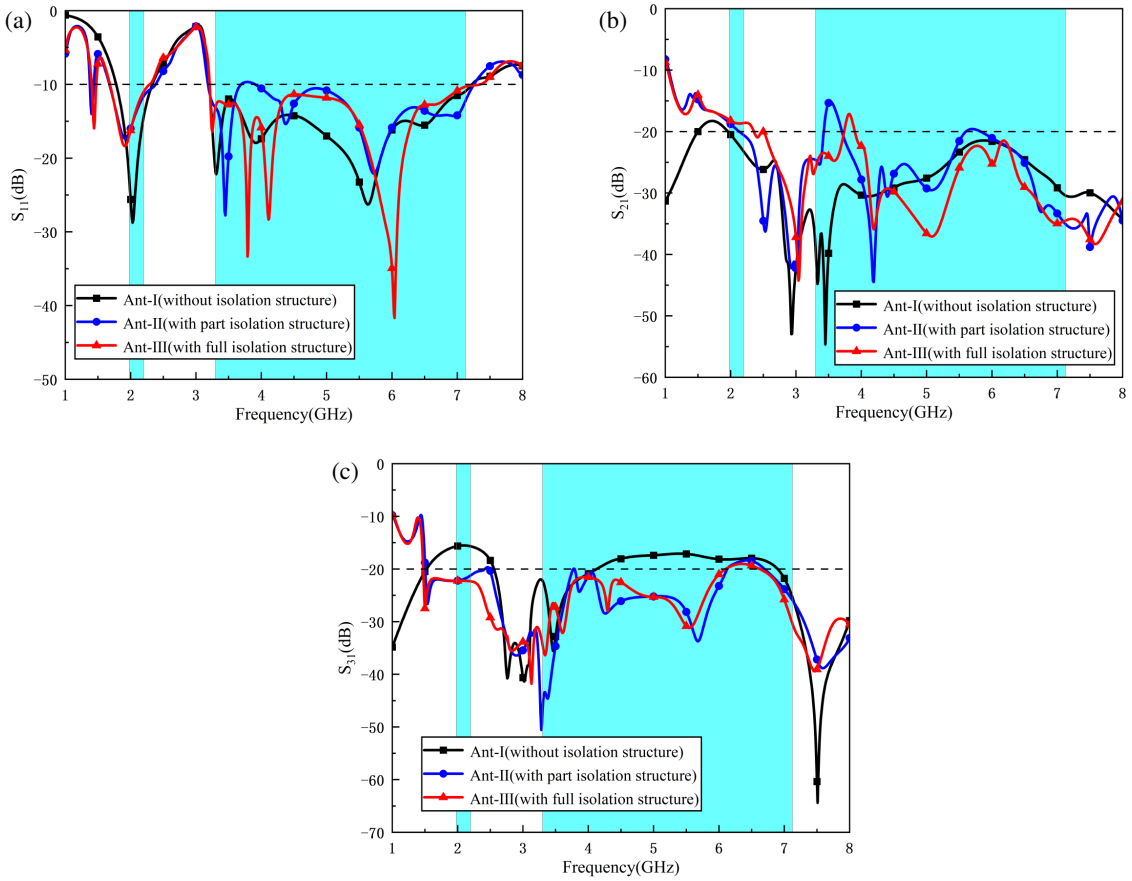

FIGURE 8. Antenna S-parameter of different isolation structures. (a) S_{11}. (b) S_{21}. (c) S_{31}.

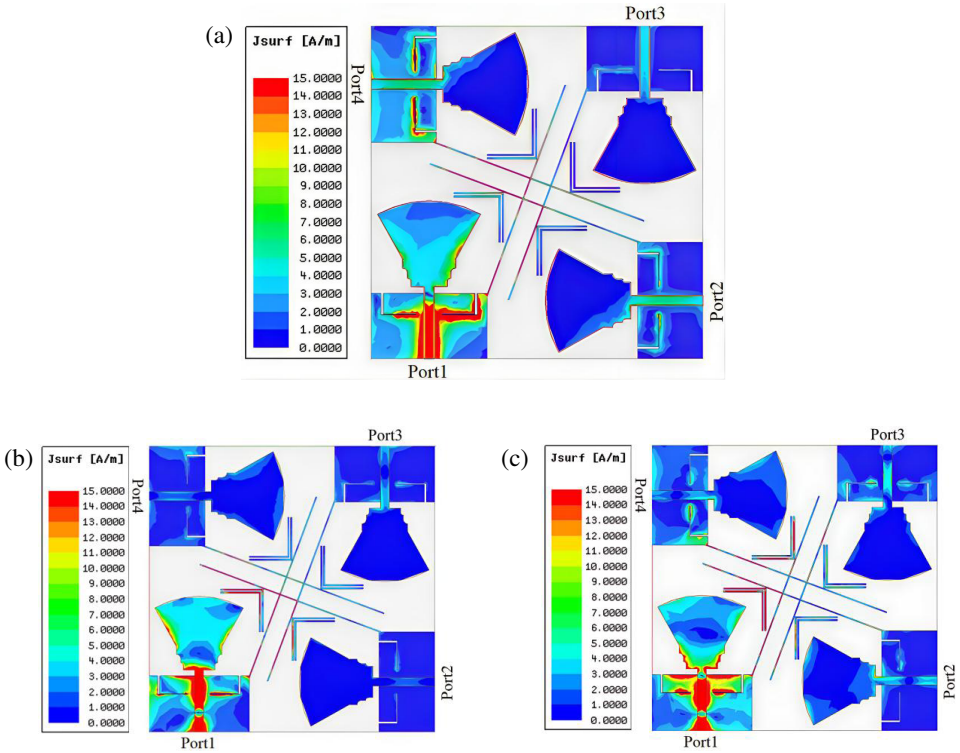

FIGURE 9. Antenna current distribution diagram. (a) 2.1 GHz. (b) 4.6 GHz. (c) 6 GHz

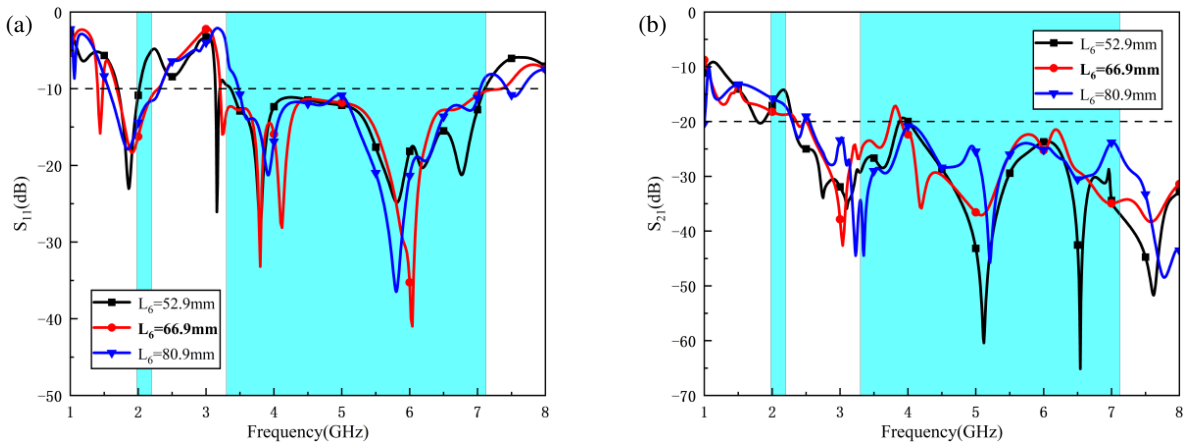

FIGURE 10. Effect of L_6 on S-parameter. (a) S_{11}. (b) S_{21}.

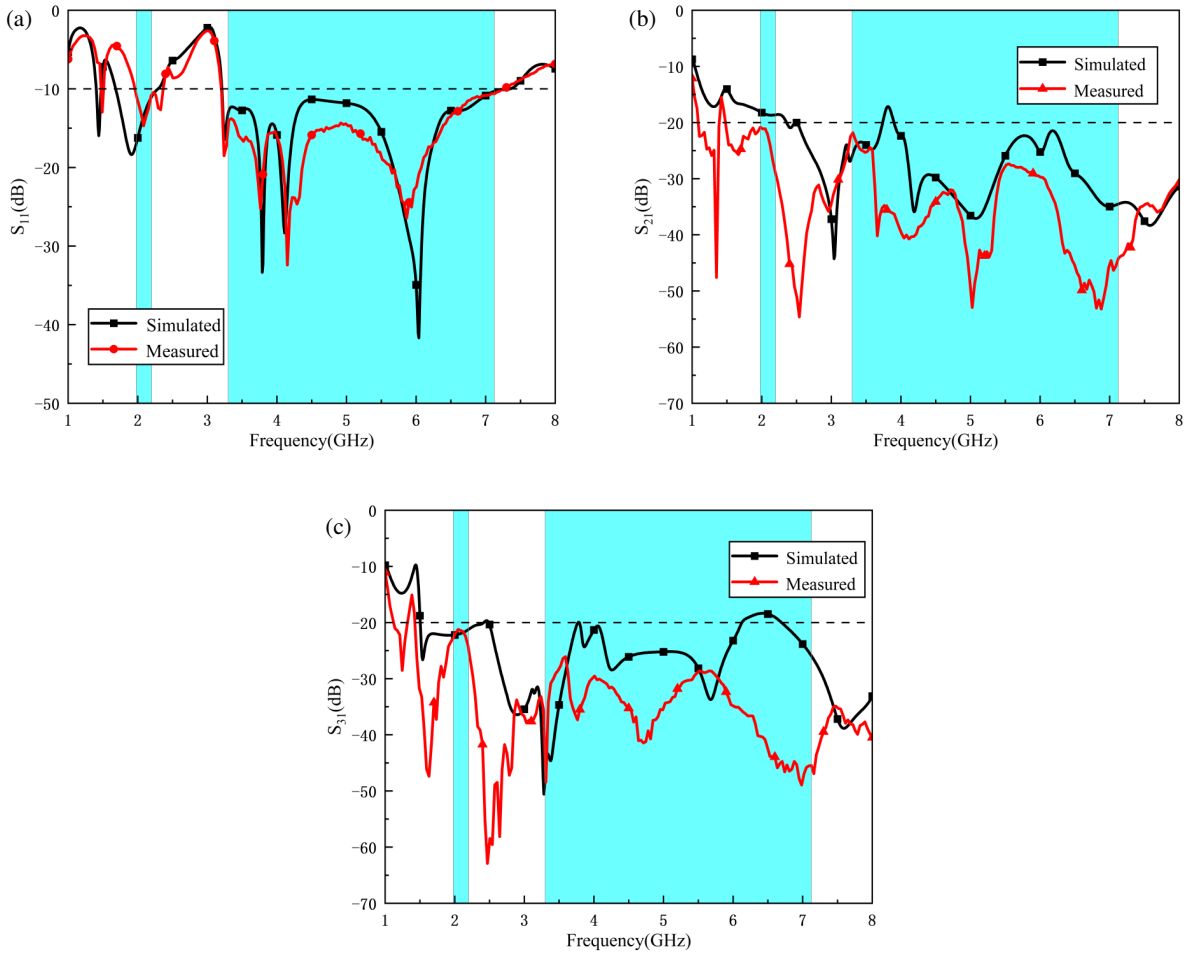

FIGURE 11. Comparison of S-parameters. (a) S_{11}. (b) S_{21}. (c) S_{31}.

ECC. The formulas for calculating ECC and DG are provided below [33]:

$$\rho_e(i,j) = \frac{\left|\iint_{4\pi} \vec{F}_i(\theta,\varphi)\cdot\vec{F}_j(\theta,\varphi)d\Omega\right|^2}{\iint_{4\pi}\left|\vec{F}_i(\theta,\varphi)\right|^2 d\Omega\cdot\iint_{4\pi}\left|\vec{F}_j(\theta,\varphi)\right|^2 d\Omega} \quad (3)$$

$$DG = 10\sqrt{1-(ECC)^2} \quad (4)$$

The F in formula (3) represents the radiation pattern function. The comparisons of the simulated and measured ECCs and DGs for the antenna are presented in Fig. 16 and Fig. 17. From the diagram, there are slight fluctuations in the measured curve of the antenna compared to the simulated data, which can still meet ECC < 0.0015 and DG > 9.9999 in the required frequency band, which satisfies the ECC and DG criteria neces-

FIGURE 12. MIMO antenna measurement setup.

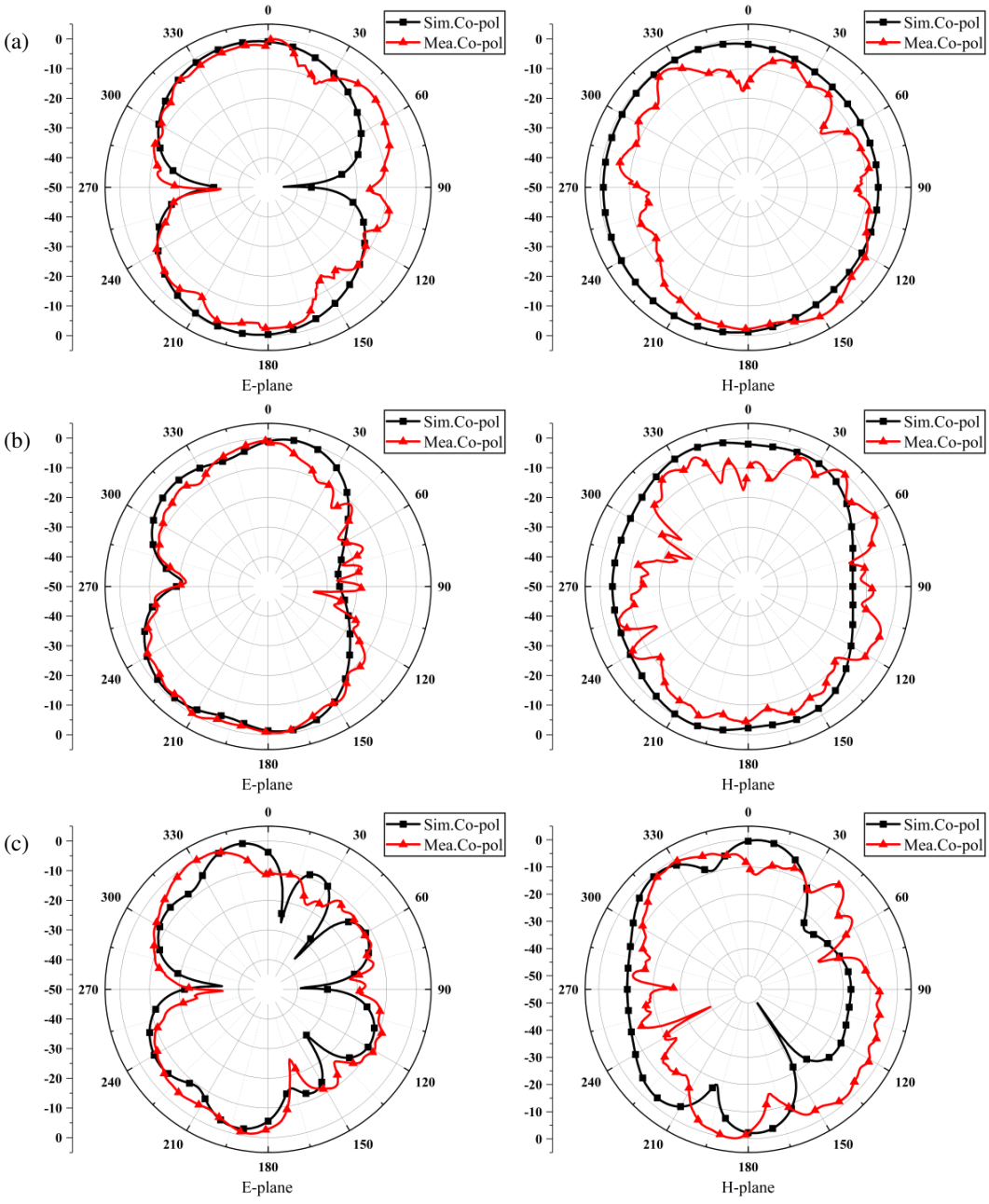

FIGURE 13. MIMO antenna radiation patterns. (a) 2.1 GHz. (b) 4.6 GHz. (c) 6 GHz.

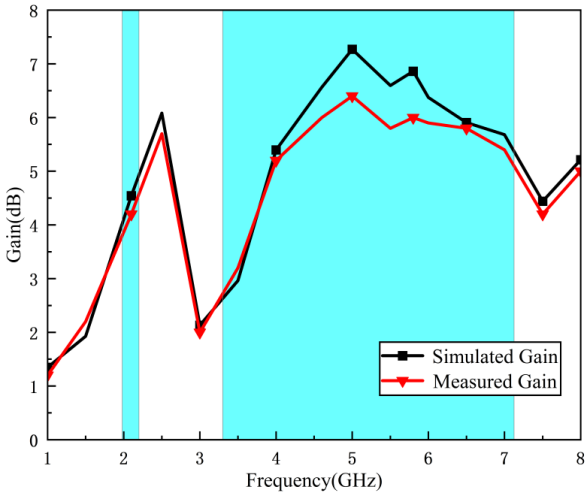

FIGURE 14. Antenna peak gain diagram.

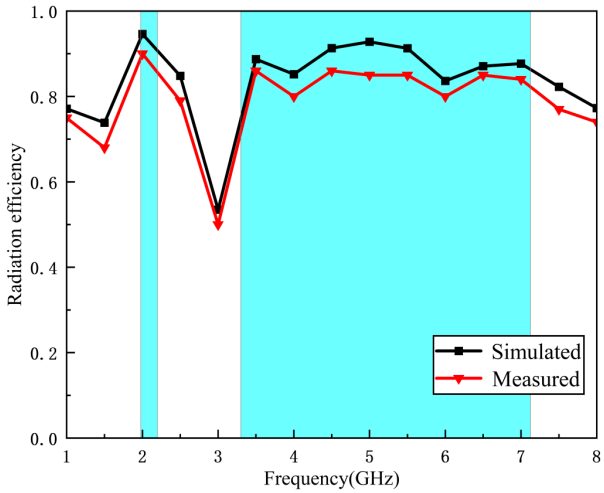

FIGURE 15. Antenna radiation efficiency.

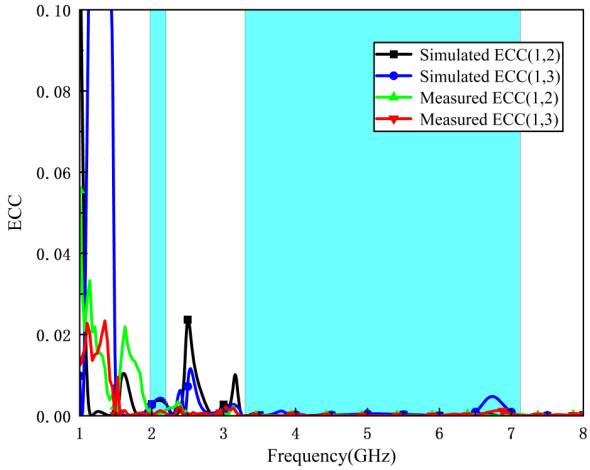

FIGURE 16. ECC of the proposed antenna.

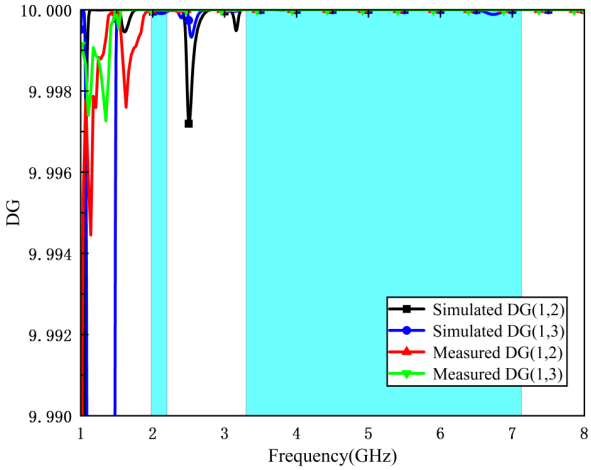

FIGURE 17. DG of the proposed antenna.

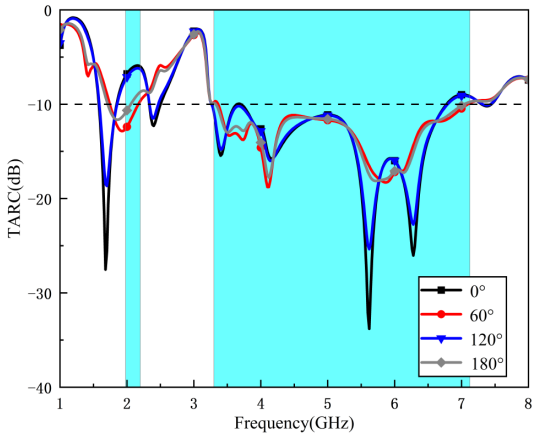

FIGURE 18. Simulated TARC of the antenna.

sary for the design of MIMO antennas. This suggests that the antenna has robust signal transmission and reception capabilities, with a high degree of channel independence in the MIMO antenna.

3.5. TARC

The total active reflection coefficient (TARC) can represent the coupling degree of the signal, which can be regarded as a measure of the radiation efficiency of multi-port antenna MIMO array. It is capable of accurately defining the antenna's radiation efficiency and impedance bandwidth, and can be computed using the following equation:

$$TARC = N^{-0.5}\sqrt{\sum_{i=1}^{N}\left|\sum_{k=1}^{N} S_{ik}e^{j\theta_{k-1}}\right|^2} \quad (5)$$

Variable θ denotes the excitation phase angle, which can take the values of 0°, 60°, 120°, and 180°. From Fig. 18, it can be seen that the curves of 0° and 120° are less than −5.9 dB at low frequency, and the remaining values are mostly below −10 dB, which signifies that the antenna offers good diversity capability.

4. PERFORMANCE COMPARISON

In Table 2, the characteristics of the designed antenna were evaluated against those of multiband MIMO antennas presented

in recent research articles. The antenna substrate material, feeding mode, working frequency band, isolation, and other parameters are compared. Although the antennas of [12, 14, 20, 26] have good isolation, they are not connected to the ground. In [22, 23], the antenna isolation is only better than 15 dB. In [27, 28, 29], the dual-band antennas only have two ports. On the whole, the four-element antenna designed in this paper has higher isolation, lower ECC (< 0.0015) , and higher DG (> 9.9999), which can be well applied to 5G satellite communication and 6G fields.

5. CONCLUSION

In this paper, a dual-band four-element MIMO antenna with a size of 100 mm $\times$ 100 mm $\times$ 1.6 mm is designed for 5G n256/n77/n78/n79 and 6G band. The dual-frequency characteristic is achieved by fan-shaped monopoles and symmetrical L-shaped grooves on the ground. The experimental results demonstrate that the antenna operates between 1.95–2.37 GHz and 3.2–7.25 GHz, with isolation levels remaining below -20 dB within the specified frequency ranges. The ECC value is below 0.0015, while the DG value exceeds 9.9999. It can be concluded that the antenna exhibits strong diversity capabilities. In addition, this antenna demonstrates good radiation properties, achieving a measured gain of 6.4 dB. The empirical results confirm that the designed MIMO antenna is suitable for the field of 5G satellite communication and 6G systems.

REFERENCES

[1] Meena, P., M. B. Pal, P. K. Jain, and R. Pamula, "6G communication networks: Introduction, vision, challenges, and future directions," *Wireless Personal Communications*, Vol. 125, No. 2, 1097–1123, 2022.

[2] Liu, R., M. Hua, K. Guan, X. Wang, L. Zhang, T. Mao, D. Zhang, Q. Wu, and A. Jamalipour, "6G enabled advanced transportation systems," *IEEE Transactions on Intelligent Transportation Systems*, Vol. 25, No. 9, 10 564–10 580, 2024.

[3] De Figueiredo, F. A. P., "An overview of massive MIMO for 5G and 6G," *IEEE Latin America Transactions*, Vol. 20, No. 6, 931–940, 2022.

[4] Islam, H., S. Das, T. Ali, T. Bose, O. Prakash, and P. Kumar, "A frequency reconfigurable MIMO antenna with bandstop filter decoupling network for cognitive communication," *Sensors*, Vol. 22, No. 18, 6937, 2022.

[5] Kormilainen, R., R. Luomaniemi, A. Lehtovuori, and V. Viikari, "A lumped-element decoupling and matching network for a four-element mobile handset MIMO antenna," *International Journal of Antennas and Propagation*, Vol. 2019, No. 1, 1934726, 2019.

[6] Li, M., Y. Zhang, D. Wu, K. L. Yeung, L. Jiang, and R. Murch, "Decoupling and matching network for dual-band MIMO antennas," *IEEE Transactions on Antennas and Propagation*, Vol. 70, No. 3, 1764–1775, 2022.

[7] Sharma, U., G. Srivastava, M. K. Khandelwal, and R. Roges, "Shorting pins-based triple band circularly polarized modified monopole compact dual-port MIMO antenna for sub-6 GHz wireless applications," *AEU — International Journal of Electronics and Communications*, Vol. 176, 155162, 2024.

[8] Naidu, P. V., D. M. Babu, S. H. Akkapanthula, A. Kumar, N. Vummadisetty, and S. Kumar, "A tri-band triangular lamp post shaped quad port MIMO antenna," *International Journal of Communication Systems*, Vol. 35, No. 9, e5131, 2022.

[9] Naidu, P. V., D. M. Babu, A. S. Haranadh, S. Kumar, A. Kumar, N. Vummadisetty, and D. Pavansai, "Design and performance analysis of 4-port trophy shaped MIMO antenna for tri-band applications," *Microsystem Technologies*, Vol. 28, No. 4, 1037–1046, 2022.

[10] Ramasamy, S. and A. Madhu, "A compact tri-band MIMO antenna for WLAN and 5G applications," *Applied Physics A*, Vol. 130, No. 2, 113, 2024.

[11] Addepalli, T., M. Sharma, M. S. Kumar, N. K. Gollamudi, P. R. Kapula, and C. M. Kumar, "Self-isolated miniaturized four-port multiband 5G sub 6 GHz MIMO antenna exclusively for n77/n78 & n79 wireless band applications," *Wireless Networks*, Vol. 30, No. 2, 1037–1053, 2024.

[12] Kansal, P., A. K. Mandpura, and N. Kumar, "A dual band CPW-fed MIMO antenna for fifth generation application," *Physica Scripta*, Vol. 99, No. 5, 055548, 2024.

[13] Mood, Y. and R. Pandeeswari, "A novel SRR metamaterial inspired CPW-fed dual band MIMO antenna for sub-6 GHz 5G application," *Wireless Personal Communications*, Vol. 130, No. 2, 1277–1293, 2023.

[14] Sree, G. N. J., K. V. Babu, S. Das, and T. Islam, "Design and optimization of a deep learning algorithm assisted stub-loaded dual band four-port MIMO antenna for Sub-6 GHz 5G and X band satellite communication applications," *AEU — International Journal of Electronics and Communications*, Vol. 175, 155074, 2024.

[15] Doloi, T., G. S. Das, P. P. Kalita, A. Buragohain, R. Devi, and Y. Beria, "A novel 4-port MIMO antenna with chamfered edge for 5G NR n77/n78/n79 bands and WLAN applications," *Physica Scripta*, Vol. 99, No. 10, 105013, 2024.

[16] Liu, R., X. An, H. Zheng, M. Wang, Z. Gao, and E. Li, "Neutralization line decoupling tri-band multiple-input multiple-output antenna design," *IEEE Access*, Vol. 8, 27 018–27 026, 2020.

[17] Pradeep, P., K. J. Sankar, and P. C. Sekhar, "A compact semi-circular slot MIMO antenna with enhanced isolation for sub-6 GHz 5G WLAN applications," *Wireless Personal Communications*, Vol. 125, No. 4, 3683–3698, 2022.

[18] Babu, K. V., S. Das, S. S. Ali, M. E. Ghzaoui, B. T. P. Madhav, and S. K. Patel, "Broadband sub-6 GHz flower-shaped MIMO antenna with high isolation using theory of characteristic mode analysis (TCMA) for 5G NR bands and WLAN applications," *International Journal of Communication Systems*, Vol. 36, No. 6, e5442, 2023.

[19] Chen, Z., J. Huang, B. Chen, and G. Liu, "Minimized dual-band MIMO antenna with high isolation for 5G and WLAN applications," *Wireless Personal Communications*, Vol. 126, No. 4, 3269–3278, 2022.

[20] Salamin, M. A., A. Zugari, M. Alibakhshikenari, C. H. See, R. Abd-Alhameed, and E. Limiti, "Compact highly isolated dual-band 4-port MIMO antenna for sub-6 GHz applications," *Journal of Electromagnetic Waves and Applications*, Vol. 37, No. 10-12, 1023–1043, 2023.

[21] John, D. M., S. Vincent, K. Nayak, B. S. Supreetha, T. Ali, P. Kumar, and S. Pathan, "A compact flexible four-element dual-band antenna using a unique defective ground decoupling structure for Sub-6 GHz wearable applications," *Results in Engineering*, Vol. 21, 101900, 2024.

[22] Addepalli, T., V. S. Nagaraju, S. Medasani, J. C. Rao, P. Badugu, C. M. Kumar, R. Uppada, and B. K. Kumar, "Four-element equilateral triangular-shaped MIMO antenna with connected ground for 5G sub: 6 GHz N79 and WiFi-6E band applications," *International Journal of Communication Systems*, Vol. 37, No. 16,

e5895, 2024.

[23] Tiwari, R. N., R. Thirumalaiah, V. R. Naidu, G. Sreenivasulu, P. Singh, and S. Rajasekaran, "Compact dual band 4-port MIMO antenna for 5G-sub 6 GHz/N38/N41/N90 and WLAN frequency bands," *AEU — International Journal of Electronics and Communications*, Vol. 171, 154919, 2023.

[24] Güler, C. and S. E. B. Keskin, "A novel high isolation 4-port compact MIMO antenna with DGS for 5G applications," *Micromachines*, Vol. 14, No. 7, 1309, 2023.

[25] Ghosh, S., G. S. Baghel, and M. V. Swati, "Design of a highly-isolated, high-gain, compact 4-port MIMO antenna loaded with CSRR and DGS for millimeter wave 5G communications," *AEU — International Journal of Electronics and Communications*, Vol. 169, 154721, 2023.

[26] Shi, C., Z. Zhao, and C. Du, "A design of quad-element dual-Band MIMO antenna for 5G application," *Micromachines*, Vol. 14, No. 7, 1316, 2023.

[27] Tiwari, R. N., P. Singh, S. Pandey, R. Anand, D. K. Singh, and B. K. Kanaujia, "Swastika shaped slot embedded two port dual frequency band MIMO antenna for wireless applications," *Analog Integrated Circuits and Signal Processing*, Vol. 109, No. 1, 103–113, 2021.

[28] Alharbi, A. G., J. Kulkarni, A. Desai, C.-Y.-D. Sim, and A. Poddar, "A multi-slot two-antenna MIMO with high isolation for sub-6 GHz 5G/IEEE802. 11ac/ax/C-band/X-band wireless and satellite applications," *Electronics*, Vol. 11, No. 3, 473, 2022.

[29] Roy, S. and U. Chakraborty, "Mutual coupling reduction in a multi-band MIMO antenna using meta-inspired decoupling network," *Wireless Personal Communications*, Vol. 114, No. 4, 3231–3246, 2020.

[30] Zhang, J., C. Du, L. Pei, and H. Liu, "A CPW-fed dual band four-port MIMO antenna based on liquid crystal polymer for flexible IoT applications," *International Journal of Microwave and Wireless Technologies*, Vol. 15, No. 9, 1570–1578, 2023.

[31] Wu, Y., W. Wang, W. Wang, and J. Ran, "Design of a tri-band multiple input multiple output antenna with high isolation for 5G applications," *International Journal of RF and Microwave Computer-Aided Engineering*, Vol. 32, No. 6, e23153, 2022.

[32] Bayarzaya, B., N. Hussain, W. A. Awan, M. A. Sufian, A. Abbas, D. Choi, J. Lee, and N. Kim, "A compact MIMO antenna with improved isolation for ISM, sub-6 GHz, and WLAN application," *Micromachines*, Vol. 13, No. 8, 1355, 2022.

[33] Peng, X. and C. Du, "A flexible CPW-fed tri-band four-port MIMO antenna for 5G/WIFI 6E wearable applications," *AEU — International Journal of Electronics and Communications*, Vol. 174, 155036, 2024.

[34] Xu, Y., P. Dong, and A. Wang, "Design of a high isolation tri-band MIMO antenna for coal mine applications," *Journal of Electromagnetic Waves and Applications*, Vol. 37, No. 13, 1106–1121, 2023.

[35] Du, C., H. Liu, X. Wang, Y. Nie, and Z. Yang, "Compact CPW-fed triple-band MIMO antenna for wireless body area network based on flexible liquid crystal polymer," *Journal of Electromagnetic Waves and Applications*, Vol. 36, No. 10, 1436–1450, 2022.